European Journal of Pharmacology 832 (2018) 11–24

Contents lists available at ScienceDirect

European Journal of Pharmacology

journal homepage: www.elsevier.com/locate/ejphar

Molecular and cellular pharmacology

# Detailed investigation of anticancer activity of sulfamoyl benz(sulfon) amides and 1*H*–pyrazol–4–yl benzamides: An experimental and computational study

Jamshed Iqbal[a,*], Syeda Abida Ejaz[a], Aamer Saeed[b], Mariya al-Rashida[c,*]

[a] Centre for Advanced Drug Research, COMSATS Institute of Information Technology, Abbottabad 22060, Pakistan
[b] Department of Chemistry, Quaid-i-Azam University, Islamabad 45320, Pakistan
[c] Department of Chemistry, Forman Christian College (A Chartered University), Lahore, Pakistan

ARTICLE INFO

*Keywords:*
Breast cancer cells (MCF–7)
Bone marrow cells (K–562)
Cervical cancer cells (HeLa)
Anti-cancer activity
Flow cytometry, DNA interaction and docking

ABSTRACT

Cancer is the second leading cause of mortality worldwide. Therapeutic approach to cancer is a multi-faceted one, whereby many cellular/enzymatic pathways have been discovered as important drug targets for the treatment of cancer. A major disadvantage of most of the currently available anticancer drugs is their non-selective cytotoxicity towards cancerous as well as healthy cells. Another major hurdle in cancer therapy is the development of resistance to anticancer drugs. This necessitates the discovery of new molecules with potent and selective cytotoxic activity towards only cancerous cells, with minimum or no damage to the normal/healthy cells. Herein we report detailed investigation into the anticancer activity of sulfamoyl benz(sulfon)amides (**1a-1g**, **2a-2k**) and 1*H*–pyrazol–4–yl benzamides (**3a-3j**) against three cancer cell lines, breast cancer cells (MCF–7), bone-marrow cancer cells (K–562) and cervical cancer cells (HeLa). For comparison, screening against healthy baby hamster kidney cells (BHK-21) was carried out. All compounds exhibited selective cytotoxicity towards cancerous cells. Cell cycle analysis was carried out using flow cytometry, followed by fluorescence microscopic analysis. DNA interaction and docking studies were also carried out.

## 1. Introduction

Cancer is among the most prevailing diseases of the current decade, with one of the highest mortality rate (Danaei et al., 2005). A variety of factors are known to contribute to cancer; many cellular/enzymatic pathways have been discovered as important drug targets for the treatment of cancer. However development of resistance in the cancerous cells to the available anticancer therapeutics is a growing concern among researchers which necessitates the discovery of new potent molecules with enhanced anticancer activity and less resistance (Dutta and Garner, 2003; Kateb et al., 2011). Currently, a variety of potent anticancer drugs are available, yet most of the drugs are cytotoxic not only to the cancerous cells but to the healthy cells as well, this results in development of severe side effects to these drugs such as weight loss, hair loss, nausea, and loss of appetite etc. (Fortin and Bérubé, 2013; Nepali et al., 2014a, 2014b; Nepali et al., 2014a, 2014b).

The sulfonamide pharmacophore is known to be biologically active exhibiting different activities such as antimicrobial (Alegaon and Alagawadi, 2012), fungicidal (Soni et al., 2010), antiviral and anti-neurodegenerative activity (Kouatly et al., 2009; Bhatt et. al, 2016). Different molecules containing sulfonamide moieties exhibit diverse biological activities including anticancer activity (Ghorab et al., 2014, 2015, 2016; Scozzafava et al., 2003). A comprehensive review by Rakesh et al. (2017) describes in detail the anticancer activities of sulfonyl and sulfonamide hybrid molecules, furthermore sulfonamides are also found to have minimum adverse effects on healthy cells. Similarly pyrazole derivatives also constitute a class of important biologically active molecules exhibiting various activities including anticancer activity (Liu et al., 2013; Faria et al., 2017). Pyrazolo[4,3-d] oxazole derivatives were found to possess anticancer as well as radiosensitizing properties (Aly and El-Gazzar, 2012).

Herein we carried out extensive studies to investigate anticancer potential of sulfamoylbenz(sulfon) amides (**1a-1g**, **2a-2k**) (al-Rashida et al., 2015) and 1*H*–pyrazol–4–yl benzamides (**3a-3j**) (Saeed et al., 2015). These compounds were screened for their cytotoxic potential against three cancer cell lines, breast cancer cells (MCF–7), bone-marrow cancer cells (K–562) and cervical cancer cells (HeLa). For comparison, screening against healthy baby hamster kidney cells (BHK-21) was also carried out, $GI_{50}$ values were determined. The results are significant since none of the compounds showed any significant cytotoxicity towards normal/healthy

* Corresponding authors.
*E-mail addresses:* drjamshed@ciit.net.pk (J. Iqbal), abidaejaz2010@gmail.com (S.A. Ejaz), aamersaeed@yahoo.com (A. Saeed), maria_al_rashida@hotmail.com (M. al-Rashida).

https://doi.org/10.1016/j.ejphar.2018.05.011
Received 23 February 2018; Received in revised form 8 May 2018; Accepted 9 May 2018

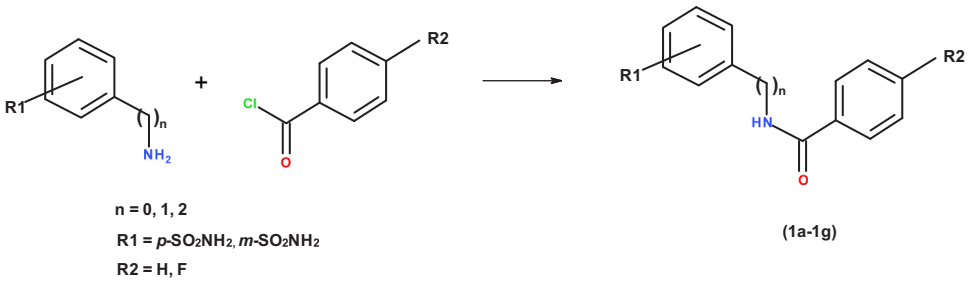


**Scheme 1.** Synthesis of sulfamoylphenyl benzamides (1a-1g).

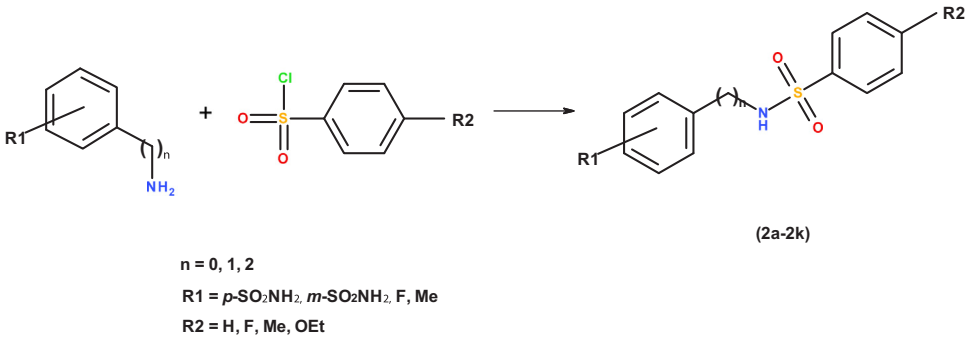


**Scheme 2.** Synthesis of sulfamoylphenyl sulfonamides (2a-2k).

**Table 1**
Purity of sulfamoylphenyl benzamides (1a-1g) and sulfamoylphenyl sulfonamides (2a-2k) derivatives through elemental analysis.

| Compound | Purity of compounds[a] |
|---|---|
| 1a | ≥ 99.6% |
| 1b | ≥ 99.8% |
| 1c | ≥ 99.9% |
| 1d | ≥ 99.6% |
| 1e | ≥ 99.7% |
| 1f | ≥ 99.9% |
| 1g | ≥ 99.9% |
| 2a | ≥ 99.8% |
| 2b | ≥ 99.6% |
| 2c | ≥ 99.7% |
| 2d | ≥ 99.9% |
| 2e | ≥ 99.8% |
| 2f | ≥ 99.6% |
| 2g | ≥ 99.7% |
| 2h | ≥ 99.9% |
| 2i | ≥ 99.8% |
| 2j | ≥ 99.9% |
| 2k | ≥ 99.8% |

[a] Purity of compounds was determined through elemental analysis.

**Table 2**
Purity of 1*H*–pyrazol–4–yl benzamides (**3a-3j**) derivatives through elemental analysis.

| Compound | Purity of compounds[a] |
|---|---|
| 3a | ≥ 99.9% |
| 3b | ≥ 99.8% |
| 3c | ≥ 99.6% |
| 3d | ≥ 99.7% |
| 3e | ≥ 99.9% |
| 3f | ≥ 99.8% |
| 3g | ≥ 99.9% |
| 3h | ≥ 99.8% |
| 3i | ≥ 99.9% |
| 3j | ≥ 99.8% |

[a] Purity of compounds was determined through elemental analysis.

cells, instead selective cytotoxicity against only cancerous cells was observed. Cell cycle progression analysis and detection of apoptotic events in different cancer cells, upon treatment with these compounds was investigated using flow cytometry. This was further complimented from results of fluorescence microscopic analysis of treated cancer cells, using two different fluorescent dyes (DAPI and PI). DNA interaction studies were carried out using UV–visible spectroscopy indicating that the compounds exhibit non-covalent groove binding to the DNA. To further rationalize binding modes, DNA docking studies were also carried out.

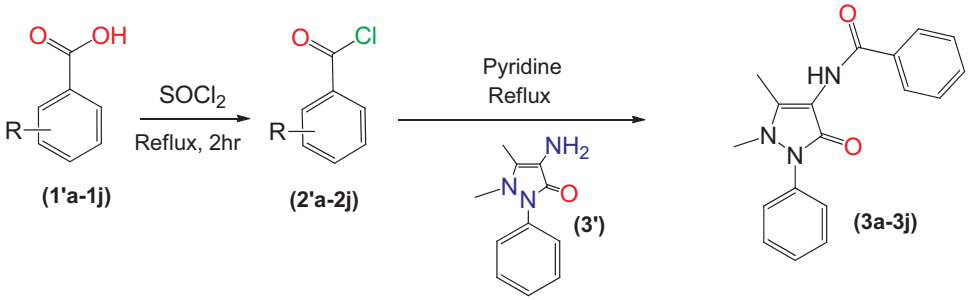


**Scheme 3.** Synthesis of pyrazole benzamide derivatives (**3a–3j**).

**Table 3**
Cytotoxic potential of sulfamoylphenyl benzamides (1a-1g), sulfamoylphenyl sulfonamides (2a-2k) and standard carboplatin against breast cancer cells (MCF–7), bone marrow lymphoblast cells (K–562), cervical cancer cells (HeLa) and normal/healthy baby hamster kidney cells (BHK–21) cell lines.

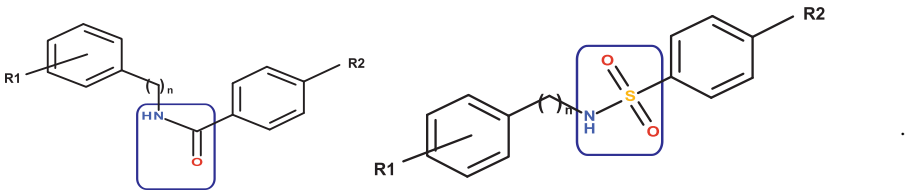


**(1a-1g)** **(2a-2k)**

| Code | n | R1 | R2 | Cytotoxic Potential (% Growth Reduction ± S.E.M) | | | |
|---|---|---|---|---|---|---|---|
| | | | | MCF–7 | K–562 | HeLa | BHK–21 |
| 1a | 0 | *p*-$SO_2NH_2$ | H | 58.5 ± 2.91 | 50.9 ± 2.67 | 70.6 ± 1.78 | 9.35 ± 0.98 |
| 1b | 1 | *p*-$SO_2NH_2$ | H | 50.5 ± 2.67 | 80.3 ± 3.21 | 69.6 ± 1.34 | 19.6 ± 2.34 |
| 1c | 2 | *p*-$SO_2NH_2$ | H | 64.7 ± 3.21 | 80.4 ± 2.87 | 68.2 ± 1.45 | 9.40 ± 0.89 |
| 1d | 0 | *p*-$SO_2NH_2$ | F | 72.7 ± 3.33 | 49.7 ± 2.11 | 56.4 ± 2.06 | 14.7 ± 1.11 |
| 1e | 1 | *p*-$SO_2NH_2$ | F | 61.3 ± 2.87 | 70.3 ± 3.09 | 89.6 ± 3.45 | 5.81 ± 1.45 |
| 1f | 2 | *p*-$SO_2NH_2$ | F | 66.2 ± 1.98 | 65.4 ± 1.98 | 70.5 ± 3.05 | 12.8 ± 1.67 |
| 1g | 0 | *m*-$SO_2NH_2$ | F | 72.2 ± 3.77 | 64.2 ± 2.67 | 60.6 ± 2.34 | 19.5 ± 2.45 |
| 2a | 0 | *p*-$SO_2NH_2$ | $CH_3$ | 61.3 ± 2.56 | 78.4 ± 2.45 | 65.2 ± 2.78 | 14.5 ± 1.45 |
| 2b | 1 | *p*-$SO_2NH_2$ | $CH_3$ | 84.7 ± 3.11 | 72.5 ± 1.98 | 63.1 ± 1.79 | 16.7 ± 1.34 |
| 2c | 2 | *p*-$SO_2NH_2$ | $CH_3$ | 54.9 ± 1.08 | 76.4 ± 3.56 | 56.3 ± 1.34 | 11.9 ± 1.08 |
| 2d | 0 | *m*-$SO_2NH_2$ | $CH_3$ | 59.1 ± 2.34 | 64.7 ± 2.15 | 54.1 ± 1.11 | 12.1 ± 1.56 |
| 2e | 0 | *p*-$SO_2NH_2$ | F | 62.1 ± 2.11 | 59.3 ± 1.78 | 34.3 ± 2.56 | 17.9 ± 2.06 |
| 2f | 1 | *p*-$SO_2NH_2$ | F | 57.3 ± 1.67 | 78.4 ± 2.24 | 79.9 ± 2.67 | 17.1 ± 2.67 |
| 2g | 2 | *p*-$SO_2NH_2$ | F | 60.2 ± 1.98 | 78.4 ± 2.98 | 77.2 ± 3.89 | 11.4 ± 1.56 |
| 2h | 0 | *m*-$SO_2NH_2$ | F | 63.6 ± 2.67 | 86.3 ± 3.67 | 56.4 ± 2.99 | 10.1 ± 1.03 |
| 2i | 0 | F | $OC_2H_5$ | 62.5 ± 2.38 | 60.7 ± 1.45 | 73.5 ± 3.25 | 13.8 ± 1.78 |
| 2j | 0 | $CH_3$ | $OC_2H_5$ | 63.1 ± 1.98 | 74.5 ± 2.08 | 59.9 ± 1.87 | 17.6 ± 1.54 |
| 2k | 0 | $CH_3$ | H | 61.7 ± 1.11 | 76.4 ± 1.78 | 69.3 ± 2.11 | 9.03 ± 1.56 |
| Carboplatin | | | | 90.7 ± 3.08 | 82.8 ± 2.67 | 85.2 ± 2.98 | 18.4 ± 2.67 |

The cytotoxic potential was measured at the final concentration of 100 μM of tested compounds. Data represents the mean values (S.E.M) for three independent determinations.

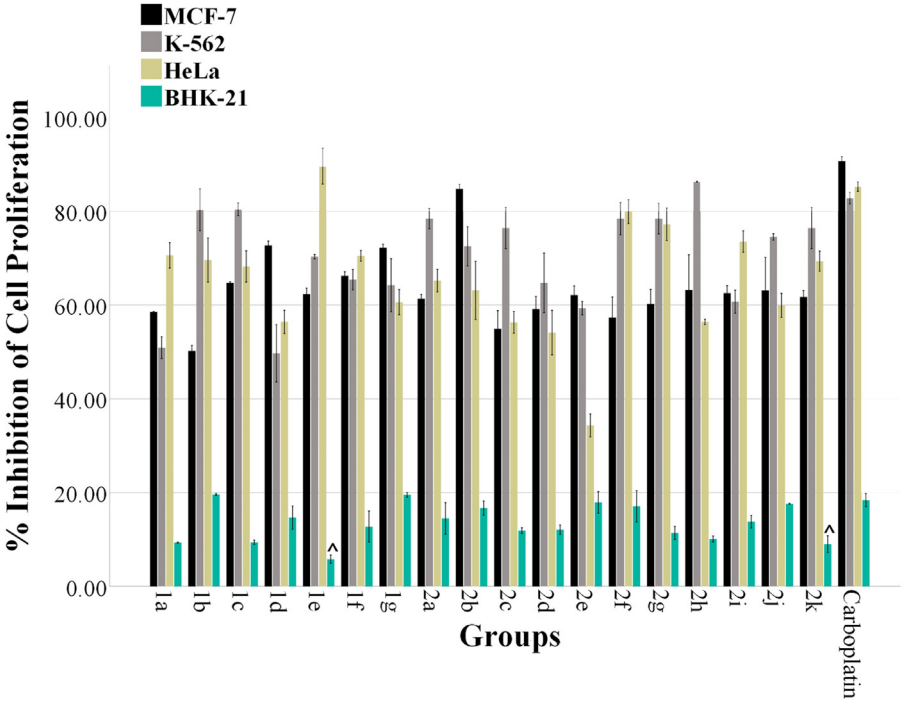


**Fig. 1.** Bar graph representation of cytotoxic potential of sulfamoylphenyl benzamides **(1a-1g),** sulfamoylphenyl sulfonamides **(2a-2k)** and standard carboplatin, against breast cancer cells (MCF–7), bone marrow lymphoblast cells (K–562), cervical cancer cells (HeLa) and normal/healthy baby hamster kidney cells (BHK–21) cell lines. All the groups in the graph are statistically significant ($P < 0.05$) using one way ANOVA except those with a cap (^).

**Table 4**
Growth inhibitory values $GI_{50}$ ± S.E.M (μM) for compounds 1e, 2b and 2h showing maximum inhibition against growth of cancerous cells MCF-7, K-562 and HeLa.

| Code | MCF–7 $GI_{50}$ ± S.E.M (μM) | K–562 | HeLa |
|---|---|---|---|
| 1e | 6.58 ± 0.63 | 19.1 ± 1.66 | 4.64 ± 0.34 |
| 2b | 0.75 ± 0.02 | 16.6 ± 1.11 | 8.09 ± 0.88 |
| 2h | 10.4 ± 1.67 | 12.2 ± 1.09 | 15.1 ± 1.77 |
| Carboplatin | 3.91 ± 0.32 | 4.11 ± 0.78 | 5.13 ± 0.45 |

$GI_{50}$ denotes compound concentrations that result in a 50% decrease in the cell number compared to non–treated controls and were derived after 24 h treatment. Results from three independent experiments are presented.

## 2. Material and methods

### 2.1. Synthesis of sulfamoylphenyl (sulfon)/benzamides and pyrazole benzamides

The sulfamoylphenyl benzamides **(1a-1g)** and sulfamoylphenyl sulfonamides **(2a-2k)** were synthesized according to our already reported method (al-Rashida et al., 2015). Similarly pyrazole benzamide derivatives **(3a-3j)** were also synthesized according to our already reported method (Saeed et al., 2015).

### 2.2. Anticancer assays

#### 2.2.1. Cell Viability Assay (MTT Assay)

The cytotoxic potential of sulfamoylphenyl benzamides **(1a-1g),** sulfamoylphenyl sulfonamides **(2a-2k)** and pyrazole benzamides **(3a-3j)** was evaluated by using MTT (dimethyl–2–thiazolyl–2, 5–diphenyl–2H–tetrazolium bromide)–based cell viability assay (Mosmann, 1983) and (Nikš, 1990). Three different cancer cell lines were used for the study *i.e.,* breast cancer cells (MCF-7), cervical cancer cells (HeLa) and bone marrow cells *i.e.,* Lymphoblast cells (K-562). The effect of the selected derivatives was also investigated against normal cells i.e. baby hamster kidney cells (BHK-21). All the cells were seeded in 96–well flat–bottom plates at a final concentration of $2.5 \times 10^4$ cells/ ml. The plates were incubated for 24 h under conditions of 5% $CO_2$ and temperature of 37 °C. The compounds were added to the respective wells at the final concentration of 100 μM and the well containing only 100 μl of culture medium without any compound was taken as blank control. Carboplatin was used as positive control against all the cell lines, at the concentration of 100 μM. After 24 h, 10 μl of MTT reagent was added to each reaction well and plates were incubated for another 4 h under the same conditions as above. At the end, the enzyme reaction was stopped by adding 100 μl of stopping reagent (50% isopropanol and 50 ml of 10% sodium dodecyl sulfate) and plates were kept at room temperature for 30 min under agitation. The absorbance was recorded at 570 nm after subtracting the background signal (690 nm), using a 96–well microplate reader (Bio–Tek ELx 800™). The experiment was performed in triplicate and the results were calculated as percent growth inhibition values with the mean of three independent values ( ± SEM). Growth inhibitory ($GI_{50}$) values of potent inhibitors (≥50%) were calculated by using a non–linear regression analysis program PRISM 5.0 (GraphPad, San Diego, California, USA).

#### 2.2.2. Cell cycle analysis assay

The effect of the most potent derivatives (having lower micro-molar $GI_{50}$ values) on the cell cycle of different cell lines was determined according to the previously reported method (Saito et al., 2010). All the cells were seeded at the final concentration of $2.5 \times 10^4$ cells/ ml, treated with 100 μM of selected compounds and were kept at 37 °C. After 24 h of incubation the treated cells were centrifuged at 3000 rpm for 3 min. The supernatant was discarded and the pallet was re-suspended in 200 μl of PBS solution having 3% FBS. After that, the cells were treated with 5 μl of propidium iodide (250 μg/ml), 5 μl of Triton X–100 (0.1%) and 25 μl of ribonuclease A (10 mg/ml). The reaction mixture was kept in dark for 1 h. The 10,000 events were observed for

**Table 5**
Cytotoxic potential of 1*H*–pyrazol–4–yl benzamides (**3a**-**3j**) and standard carboplatin against breast cancer cells (MCF–7), bone marrow lymphoblast cells (K–562), cervical cancer cells (HeLa) and normal/healthy baby hamster kidney cells (BHK–21) cell lines.

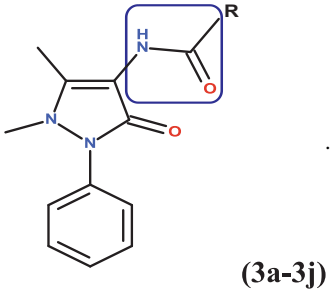


**(3a-3j)**

| Code | R | Cytotoxic Potential (% Growth Reduction ± S.E.M) | | | |
|---|---|---|---|---|---|
| | | MCF–7 | K–562 | HeLa | BHK–21 |
| 3a | Phenyl | 65.1 ± 2.76 | 80.4 ± 3.67 | 72.1 ± 2.87 | 4.18 ± 0.34 |
| 3b | 2-Methylphenyl | 50.9 ± 2.98 | 66.2 ± 2.67 | 77.6 ± 3.89 | 17.3 ± 1.09 |
| 3c | 4-Methylphenyl | 66.5 ± 3.78 | 84.3 ± 3.78 | 70.2 ± 2.78 | 29.7 ± 2.67 |
| 3d | 2-Chlorophenyl | 59.8 ± 2.87 | 9.81 ± 0.98 | 58.9 ± 1.78 | 9.43 ± 0.78 |
| 3e | 4-Chlorophenyl | 61.3 ± 3.12 | 90.2 ± 2.78 | 66.1 ± 2.56 | 5.97 ± 0.56 |
| 3f | 2-Bromophenyl | 42.4 ± 2.06 | 98.1 ± 2.89 | 66.1 ± 1.89 | 13.1 ± 1.58 |
| 3g | 3,5-Dihydroxyphenyl | 60.2 ± 2.78 | 5.88 ± 0.56 | 67.3 ± 1.67 | 4.79 ± 0.23 |
| 3h | Benzyl | 69.4 ± 3.89 | 60.8 ± 1.89 | 69.6 ± 1.78 | 10.1 ± 1.45 |
| 3i | 2-Furanyl | 76.6 ± 2.98 | 56.5 ± 2.06 | 49.2 ± 2.56 | 15.2 ± 2.16 |
| 3j | Methyl | 55.5 ± 3.16 | 70.6 ± 1.89 | 72.3 ± 3.78 | 13.1 ± 2.78 |
| Carboplatin | | 90.7 ± 3.08 | 82.8 ± 2.67 | 85.2 ± 2.98 | 18.4 ± 2.67 |

The cytotoxic potential was measured at the final concentration of 100 μM of tested compounds. Data represents the mean values (S.E.M) for three independent determinations.

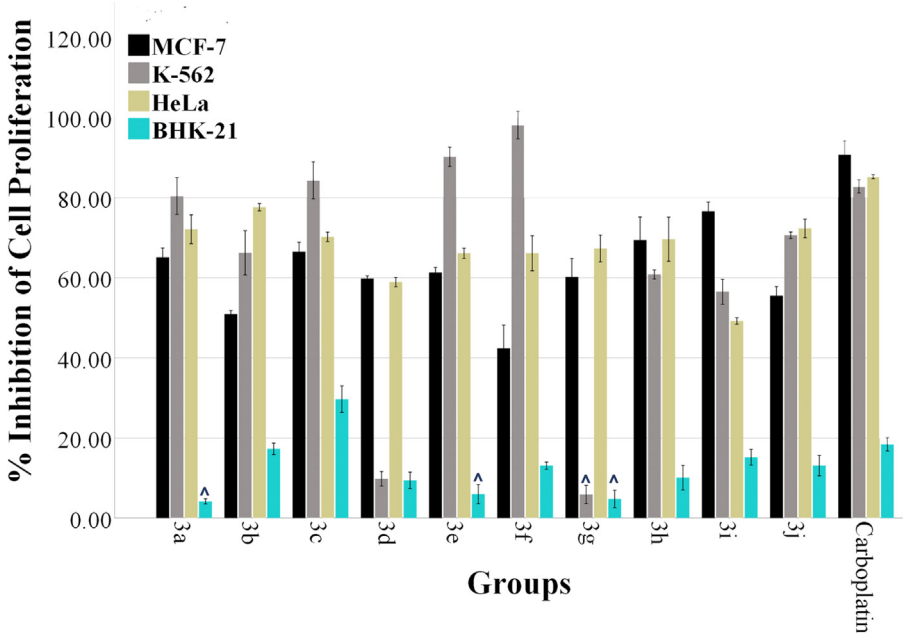


**Fig. 2.** Bar graph representation of cytotoxic potential of 1*H*–pyrazol–4–yl benzamides (**3a-3j**) and standard carboplatin, against breast cancer cells (MCF–7), bone marrow lymphoblast cells (K–562), cervical cancer cells (HeLa) and normal/healthy baby hamster kidney cells (BHK–21) cell lines. All the groups in the graph are statistically significant ($P < 0.05$) using one way ANOVA except those with a cap (^).

**Table 6**
Growth inhibitory values $GI_{50}$ ± S.E.M (μM) for compounds 3b, 3 f and 3i showing maximum inhibition against growth of cancerous cells MCF-7, K-562 and HeLa.

| Code | MCF–7 $GI_{50}$ ± S.E.M (μM) | K–562 | HeLa |
|---|---|---|---|
| 3b | 21.5 ± 2.11 | 12.1 ± 1.11 | 3.26 ± 0.03 |
| 3f | > 100 | 7.27 ± 0.48 | 8.22 ± 0.78 |
| 3i | 4.18 ± 0.01 | 18.4 ± 1.99 | > 100 |
| Carboplatin | 3.91 ± 0.32 | 4.11 ± 0.78 | 5.13 ± 0.45 |

$GI_{50}$ denotes compound concentrations that result in a 50% decrease in the cell number compared to non–treated controls and were derived after 24 h treatment. Results from three independent experiments are presented.

each sample by using the BD accuri Flow Cytometer and the analysis was done by using BD Accuri software.

### 2.2.3. Microscopic analysis of apoptosis

In order to support the results obtained from flow cytometry, the fluorescence microscopic analysis of the cells after treatment with most active compounds was carried out according to the previously reported method (Ban et al., 2014). The confluent cells with the density of $2 \times 10^5$ cells/well were treated with 100 μM of test compound and kept in $CO_2$ incubator at 37 °C for 24 h. Next day, the medium was discarded and cells were washed three times with cold PBS. Then the cells were fixed with 4% formalin and allowed to become permeable with 0.1% Triton X–100. After 5 min room incubation, 10 μl of DAPI (0.1 mg/ml) or PI (0.1 mg/ml) dye was added to stain the nuclear material and the glass slides were kept in dark for 10 min. The images were captured by using the fluorescence microscope at excitation/emission wavelength of 350/460 nm and 493/632 for DAPI and PI, respectively.

### 2.2.4. DNA interaction studies

The DNA interaction studies of the most potent compounds were performed according to the previously reported method (Sirajuddin et al., 2014). For this purpose 100 μM of each selected compound was interacted with the different concentrations of salmon sperm DNA *i.e.,* 0, 40, 90, 140, 190, 240, 290 and 340 μM obtained from the molar absorption coefficient of 6600 $M^{-1}$ $cm^{-1}$ *i.e.,* $4.15 \times 10^{-4}$ M. The same amount of DNA was also added to their respective reference solutions. The plates were kept at room temperature for 30 min. The absorption spectra were measured with blank correction using 96–well plates of 5.5 mm path length and the mode of interaction of compounds was determined by using Omega– Data Analysis Software, Program Version: 3.00 R3.

### 2.2.5. DNA docking

The binding orientation of compounds with DNA was investigated by molecular operating environment (MOE) by Chemical Computing Group Inc (MOE, version, 2014) and LeadIT. The compound structures were drawn using builder tool of MOE 2014.09. Furthermore the 3D structures of compounds were energy minimized and optimized through semi-empirical method PM3 inbuilt in MOE. The X-ray crystallographic DNA structure was obtained from Protein Data Bank (PDB IDs: 1BNA and 127D) (Drew et al., 1981). The structure of DNA was 3D protonated with its standard geometry; followed by energy optimization tool using MOPAC 7.0. Whole DNA structure was used to search for ideal conformation at default parameters with root mean squared (RMS) gradient of 0.01 $kcalmol^{-1}$. Total 100 poses per compound were generated. The best conformation was selected and then imported to Discovery Studio Visualizer (Visualizer, 2005) for visualization purpose.

## 3. Results

### 3.1. Chemistry

#### 3.1.1. Synthesis of sulfamoylphenyl benzamides and sulfamoylphenyl sulfonamides

Sulfamoylphenyl benzamides **(1a-1g)** were synthesized by reacting different aminobenzenesulfonamides with benzoyl chlorides (Scheme 1), and sulfamoylphenyl sulfonamides **(2a-2k)** were synthesized by reacting different aminobenzenesulfonamides with sulfonyl chlorides (Scheme 2) as previously reported by us (al-Rashida et al., 2015).

The purity of synthesized compounds was determined through elemental analysis as shown in Table 1 (al-Rashida et al., 2015).

#### 3.1.2. Synthesis of 1H–Pyrazol–4–yl benzamides derivatives

The synthetic pathway leading to the formation of 1*H*–pyrazol–4–yl benzamides (**3a–3j**) is depicted in Scheme 3. Firstly, the aromatic carboxylic acids (**1′a–1′j**) were refluxed with thionyl chloride to prepare respective acid halides (**2′a–2′j**), in the second step the obtained acid halides were further reacted with the 4–aminophenazone (**3′**) to afford

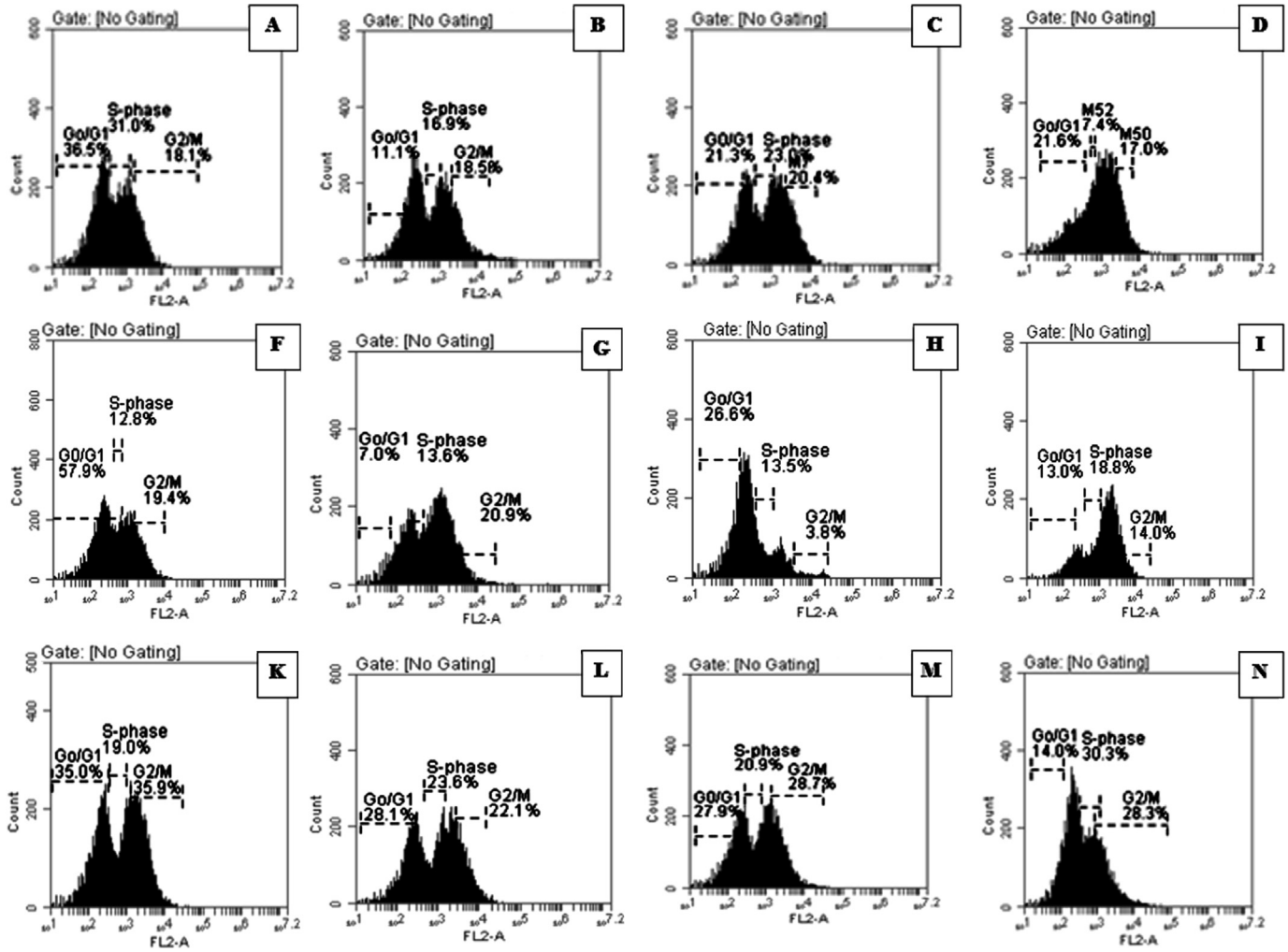


**Fig. 3.** Cell cycle analysis using propidium iodide (PI) DNA staining and flow cytometry. Data showing cell population in G0/G1, S and G2/M phases of the cell cycle (A) untreated MCF–7 cells, (B) carboplatin against MCF–7, (C) Compound **2b** against MCF–7, (D) Compound 3i against MCF–7, (E) untreated K–562 cells, (F) carboplatin against K–562, (G) Compound 2 h against K–562, (H) Compound 3f against K–562, (I) untreated HeLa cells, (J) Carboplatin against HeLa, (K) Compound **1e** against HeLa, **(L)** Compound **3b** against HeLa.

the desired pyrazole benzamide derivatives (**3a–3j**) (Saeed et al., 2015).

The purity of synthesized compounds was determined through elemental analysis as shown in table (Saeed et al., 2015).

### 3.2. Evaluation of anticancer activity

#### 3.2.1. Cytotoxic potential by MTT assay

*In vitro* evaluation of anticancer activity of all compounds **1a-1g, 2a-2k** and **3a-3j** was carried out using the 3–(4,5–dimethylthiazol–2–yl)–2,5–diphenyltetrazolium bromide (MTT) assay (Mosmann, 1983; Nikš, 1990). The cell viability was determined by measurement of purple formazan that was formed after metabolization of original yellow colored tetrazolium bromide (MTT). This conversion of yellow tetrazolium bromide to purple formazan is brought about by oxidoreductase enzymes that are typically present in the cytosol of living cells, thereby providing an estimate of number of viable (healthy (control) and cancerous) cells present after treatment with test compounds. The screening of all the derivatives was carried out using breast cancer cells (MCF-7), cervical cancer cells (HeLa) and bone marrow cells i.e., lymphoblast cells (k-562), in comparison to normal cell line i.e. baby hamster kidney cells (BHK-21). The viability of cells was assessed after 24 h treatment with 100 μM concentration of respective derivative. The cytotoxic potential was measured at the final concentration of 100 μM of tested compounds. The obtained results are expressed as percentage of viability stated in untreated cells and are presented in Table 3 and Fig. 1.

Most potent compounds were further evaluated for the determination of $GI_{50}$ values against MCF–7, K–562 and HeLa cells. The anticancer potency of the compounds was calculated by linear regression analysis of the concentration–response curves obtained for each compound (Table 4).

Similar to the results obtained for previous compounds (**1a-1g**, **2a-2k**), all 1*H*–pyrazol–4–yl benzamides (**3a-3j**) also did not inhibit growth of normal/healthy baby hamster kidney cells (BHK–21) (Table 5). Fig. 2 shows anticancer potential of these compounds in the form of a bar graph.

Most potent compounds were further evaluated for the determination of $GI_{50}$ values against MCF–7, K–562 and HeLa cells. The anticancer potency of the compounds was calculated by linear regression analysis of the concentration–response curves obtained for each compound (Table 6).

#### 3.2.2. Cell cycle analysis and detection of apoptosis in different cell lines by flow cytometry

In order to investigate the effect of most potent compounds on cell cycle progression and apoptosis, flow cytometric analysis was carried out using human breast cancer cell line (MCF–7), bone marrow lymphoblast cell lines (K–562) and human cervical cancer cell line (HeLa). The results after 24 h treatment of cells are shown in Figs. 3 and 4.

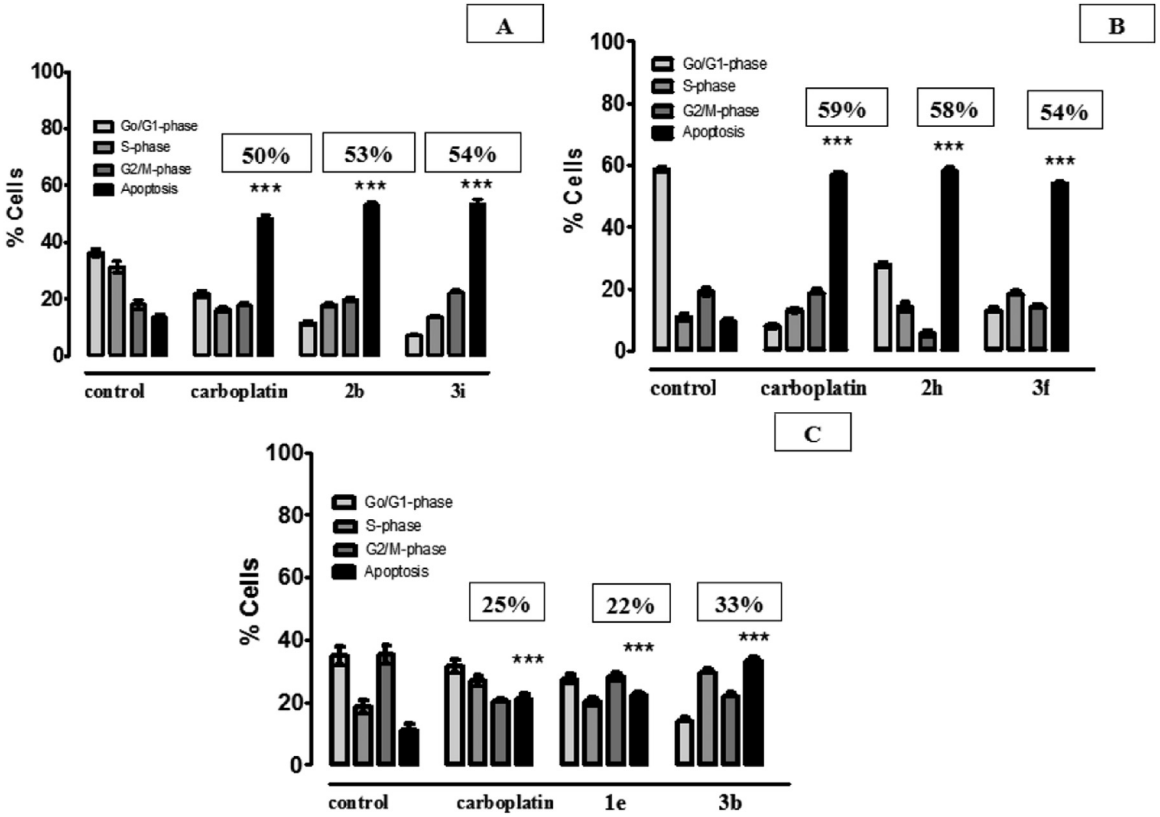


**Fig. 4.** Apoptosis induced by the most potent compounds in different cell lines (A) Compound **2b** and **3i** against MCF–7 (B) Compound **2h** and **3f** against K–562 (C) Compound **1e** and **3b** against HeLa. Data were analyzed by one way analysis of variance (ANOVA) using PRISM 5 (GraphPad).

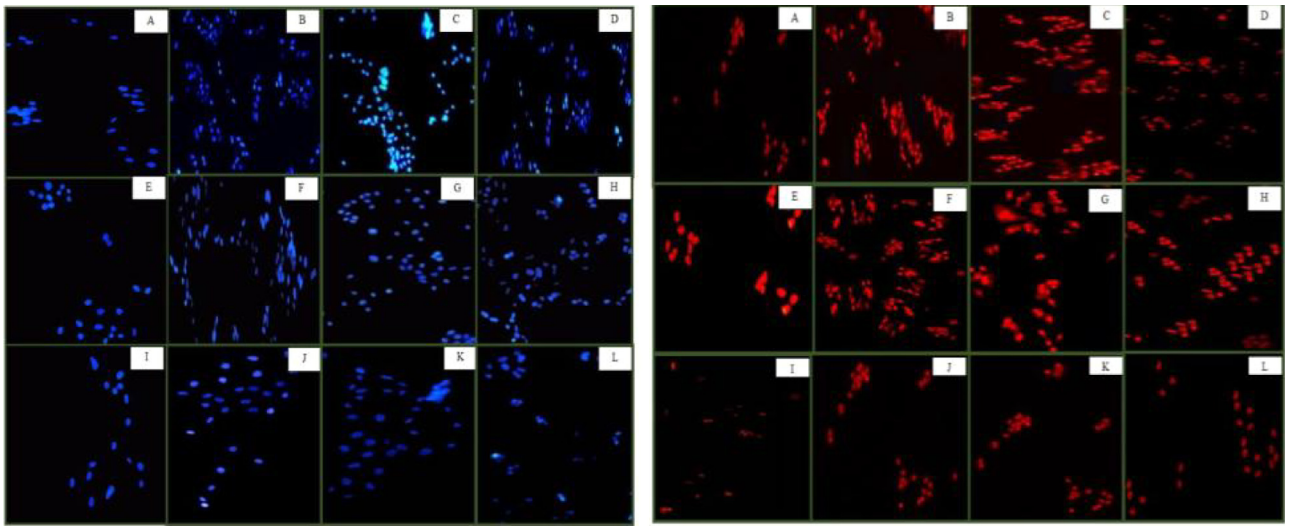

**Fig. 5.** Cell apoptosis observed under fluorescence microscope using DAPI (a; left, blue), and PI (b; right, red) staining respectively. In both (a) and (b), (A) untreated MCF–7 cells (B) carboplatin against MCF–7 (C) Compound **2b** against MCF–7 (D) Compound **3i** against MCF–7 (E) untreated K–562 cells (F) carboplatin against K–562 (G) Compound 2h against K–562 (H) Compound **3f** against K–562 (**I**) untreated HeLa cells (**J**) carboplatin against HeLa (**K**) Compound **1e** against HeLa (**L**) Compound **3b** against HeLa. In comparison to negative control, the compounds exhibited chromatin condensation, nuclear fragmentation and apoptotic body formation.

Carboplatin was used as positive control and also treated at final concentration of 100 μM. Untreated cells, MCF–7, K–562 or HeLa in the G0/G1, S and G2/M phases were considered 100% (control). The different cell cycle phases of the treated derivatives were analyzed and the percentages of G0– G1, S, and G2/ M phase cells are presented graphically in Figs. 3 and 4.

*3.2.3. Microscopic analysis of potent derivatives (using DAPI & PI)*

The most potent anti-cancer compounds (**2b, 3i, 2h, 3f, 1e** and **3b**) and carboplatin (positive control) were treated with respective cancer cell lines at final concentration of 100 μM. After 24 h, the images revealed the characteristic apoptotic changes like higher percentage of rounded cells, condensed and fragmented nuclei unlike untreated control. Fluorescent microscopic analysis was carried out to confirm the nuclear fragmentation using nuclear staining dyes (DAPI, PI). The nuclei in the viable cells have a regular, oval shape with homogeneous chromatin, whereas in the apoptotic cells, shrinking and fragmentation of the nuclei could be observed (Fig. 5(a, b)).

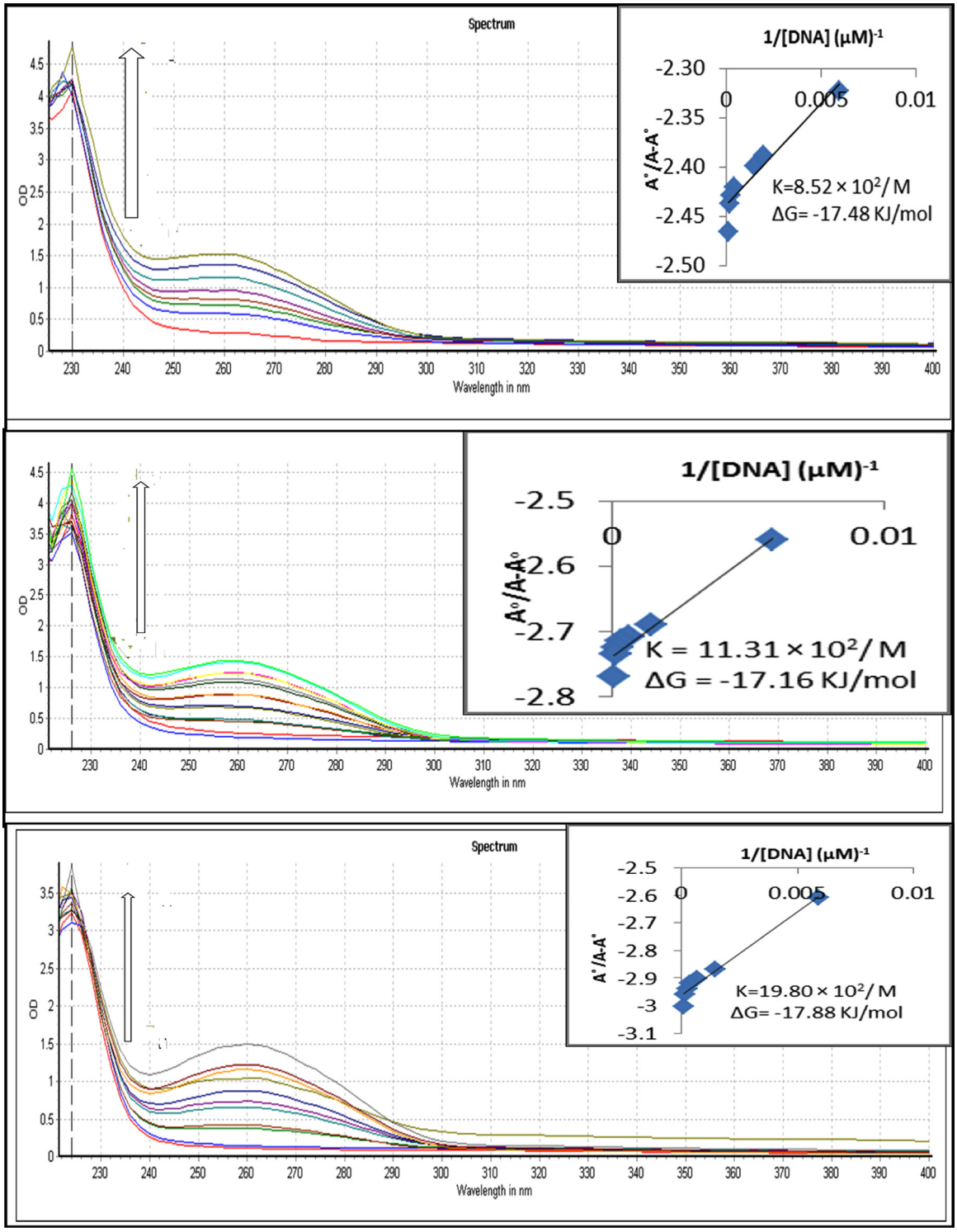


**Fig. 6.** Absorption spectra of 40 μM of (a) **2b**, **2h** and **1e** in absence and presence of 40 μM, 90 μM, 140 μM, 190 μM, 240 μM, 290 μM and 340 μM SS-DNA. The arrow direction indicates increasing concentration of DNA. The inset graph is the plot of A°/ (A–A°) vs 1/[DNA] for the determination of binding constant and Gibb's free energy of compound–DNA adduct.

### *3.2.4. DNA interaction studies*

The mechanism of action of the cytotoxic compounds against MCF–7 cells (**2b, 3i**), K–562 cells (**2h**, **3f**) and HeLa cells (**1e**, **3b**) was further evaluated by their interaction studies with SS–DNA in UV–visible range, using Omega FLUOstar, microplate reader. The absorption spectra of test compounds in the absence and presence of increasing concentration of SS–DNA was observed as depicted in Figs. 6 and 7.

### *3.2.5. DNA docking studies*

From the results of DNA interaction via UV–visible spectroscopy, it was found that all compounds were interacting with DNA as groove binders In order to rationalize these binding modes, DNA docking studies were carried out according to our previously reported protocol (al-Rashida and Ahsen, 2015). Crystal structure of DNA co-crystallized with Hoechst (minor groove binder) was downloaded from the Protein Data Bank (PDB ID 127D). Docking studies were carried out using

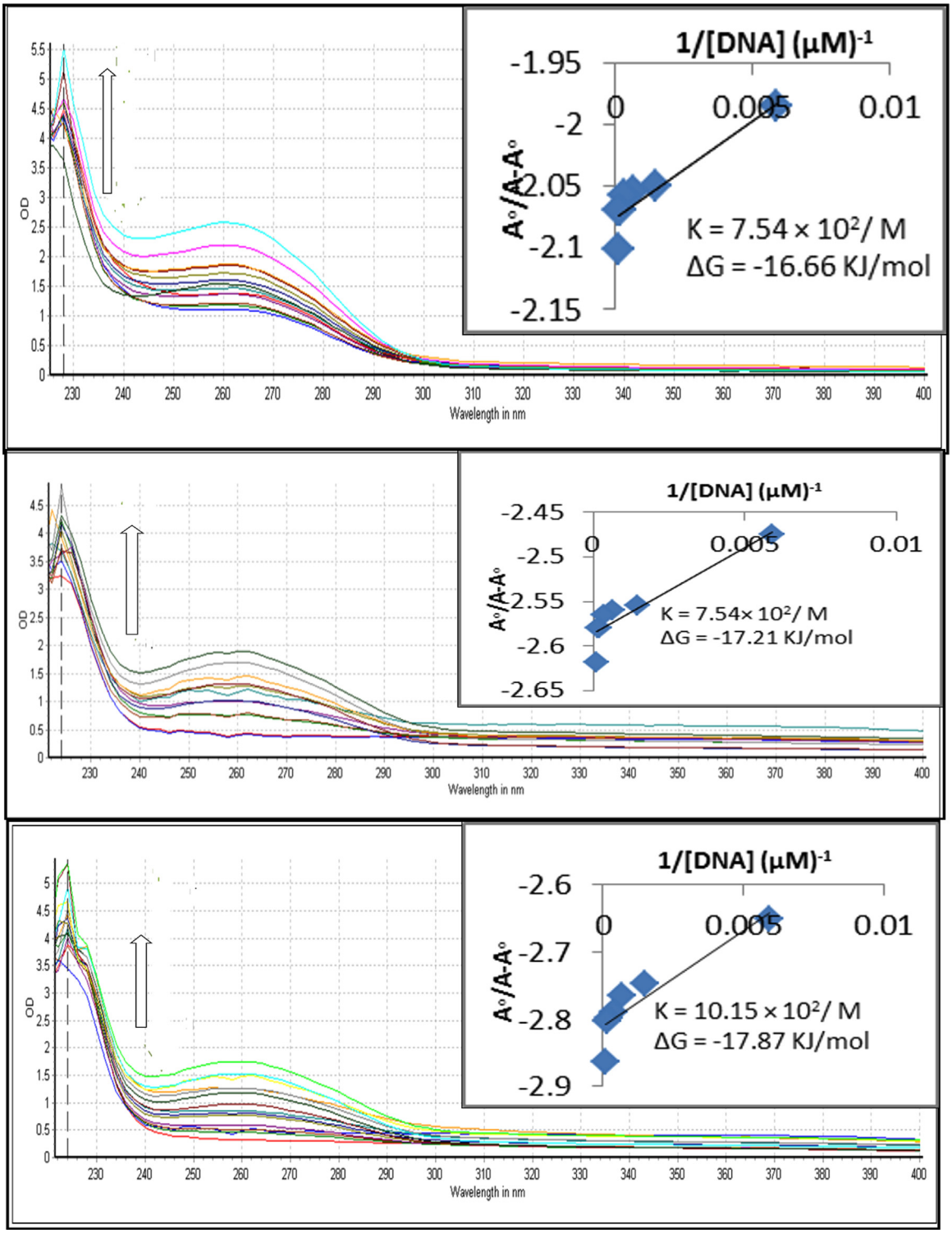


**Fig. 7.** Absorption spectra of 40 μM of (a) **3i**, **3f** and **3b** in absence and presence of 40 μM, 90 μM, 140 μM, 190 μM, 240 μM, 290 μM and 340 μM SS-DNA. The arrow direction indicates increasing concentration of DNA. The inset graph is the plot of A°/ (A–A°) vs 1/[DNA] for the determination of binding constant and Gibb's free energy of compound–DNA adduct.

BioSolveIT's LeadIT software (LeadIT, 2014). In order to validate the docking protocol, the original co-crystallized ligand, Hoechst was re-docked into the same DNA, the docking protocol was able to reproduce the experimentally observed bound conformation with rmsd of 0.99 Å. Figs. 8 and 9 show docked conformations of compounds **2b**, **2h** and **1e**, all showing DNA groove binding, which is in agreement with the experimental DNA interaction studies (Fig. 8).

Similar results were obtained from docking of 1*H*–pyrazol–4–yl benzamides **3i**, **3f** and **3b**, as shown in Figs. 10 and 11.

## 4. Discussion

The sulfonamide moiety is a highly active pharmacophore and is responsible for a number of biological activities. Sulfamoylphenyl

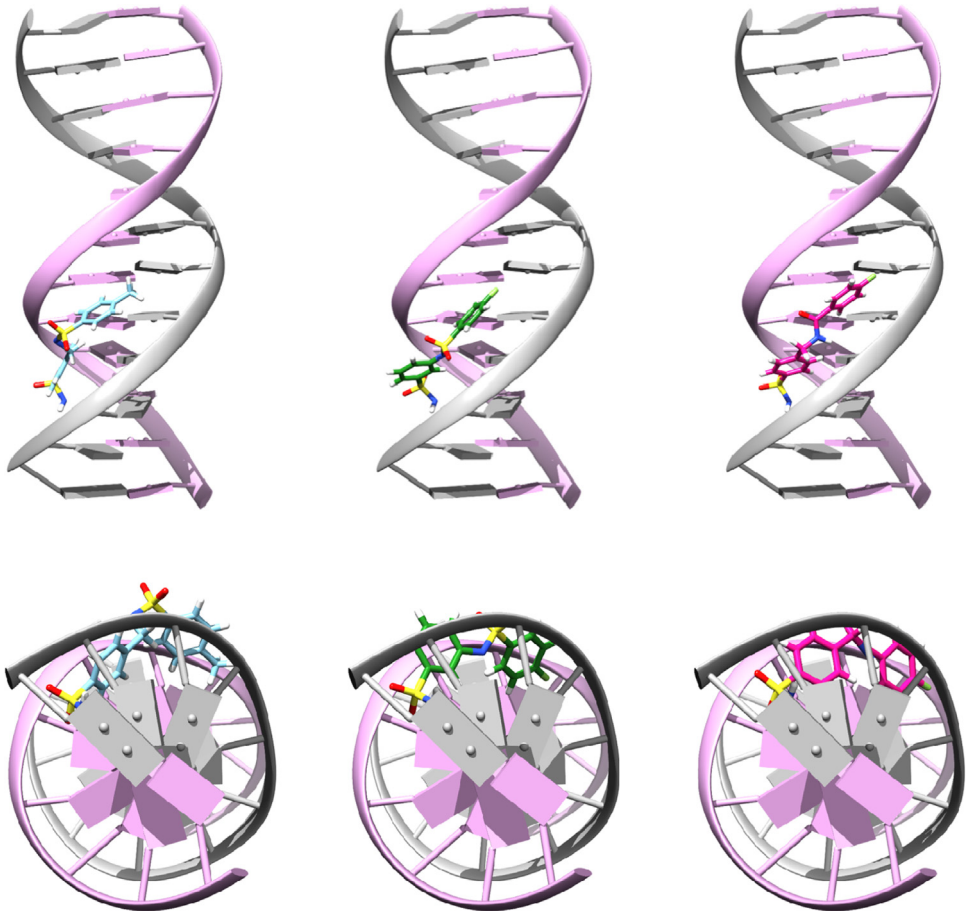

**Fig. 8.** Docked conformations of **2b** (blue), **2h** (green) and **1e** (pink), indicating DNA groove binding mode.

benzamides (**1a-1g**) and sulfamoylphenyl sulfonamides (**2a-2k**) were synthesized by reacting different aminobenzenesulfonamides with benzoyl chlorides and sulfonyl chlorides respectively (Schemes 1 and 2), as previously reported by us al-Rashida et al. (2015). The pyrazole benzamide derivatives (**3a–3j**) were synthesized via a two-step process starting with preparation of aroyl chlorides from their respective carboxylic acids, and further reaction of obtained aroyl chlorides with 4–aminophenazone as reported by us Saeed et al. (2015).

The cytotoxic potential of all compounds was evaluated using MTT assay. By virtue of this test, cellular metabolic activity can be assessed, hence it provides a means to determine cell viability. MTT (dimethyl–2–thiazolyl–2,5–diphenyl–2H–tetrazolium bromide), is a yellow colored tetrazolium dye that is taken up by cells via endocyctosis. In living cells, the NADPH dependent mitochondrial dehydrogenases reduce yellow MTT to purple colored formazan, which is determined spectrophotometrically. Since mitochondrial activity is only present in living cells, MTT test is a reliable indicator of cell viability. The viability of cells 24 h after treatment with test compounds, at concentration of 100 μM, was assessed against three different cancer cell lines i.e., breast cancer cells (MCF-7), cervical cancer cells (HeLa) and bone marrow cells i.e., Lymphoblast cells (K-562). The effect against normal cells i.e. baby hamster kidney cells (BHK-21) was also determined. All compounds with the exception of compound **2e** showed more than 50% growth inhibition of cancerous cells (Table 1). Against breast cancer cells (MCF-7), compound **2b** showed maximum inhibition of 84%, followed by compounds **1d** and **1g** exhibiting 72% growth inhibition. Third most active compound was **1f,** showing 66% inhibition. Whereas least growth inhibition was exhibited by compound **1b**, showing only 50% inhibition.

Against bone marrow lymphoblast cells (K–562), compound **2h** showed maximum growth inhibition of 86% which is slightly higher than the inhibition shown by standard carboplatin (82%). Compounds **1b** and **1c** showed 80% inhibition, followed by compounds **2a**, **2f** and **2g** exhibiting 78% growth inhibition. Compound **1d** showed least inhibition of 49.7%. Against cervical cancer cells (HeLa), maximum growth inhibition of 89% was shown by compound **1e,** it is important to note here that the inhibition shown by **1e** is higher than that of carboplatin (85%). Compounds **2f** and **2g** exhibited 79% and 77% inhibition respectively. Least inhibition was shown by compound **2e** which showed less than 50% inhibition (34%).

Most interestingly, all compounds showed no inhibition of growth (less than 19%) against normal/healthy baby hamster kidney cells (BHK–21). In the search of new potent anticancer agents, one of the most desirable trait is their ability to selectively target only cancerous cells, ideally without damaging normal or healthy cells, or (less ideally) with minimum damage to the healthy cells. In this respect, compound **1e** has emerged as the most promising candidate as a lead compound for further development of anticancer compounds from this class of compounds (Table 2). Compound **1e** exhibited maximum inhibition of 89% against cervical cancer cells (HeLa) with minimum damage (5% inhibition) to normal healthy cells (BHK–21). Against bone marrow lymphoblast cells (K–562), compound **2h** was most active (86% growth inhibition), with minimum damage to healthy cells (only 10% growth inhibition). Against breast cancer cells (MCF–7), most promising compound was **2b** (84% growth inhibition) with minimum damage to healthy cells (only 16% growth inhibition) (Fig. 1).

The results of cytotoxic activity for 1*H*–pyrazol–4–yl benzamides (**3a-3j**) are given in Table 3. Against the breast cancer cells (MCF–7), maximum growth inhibition was exhibited by compound **3i** (76%), followed by compound **3h** which showed 69% inhibition. Compounds **3a** and **3c** showed growth inhibition of 65% and 66% respectively. Against bone marrow lymphoblast cells (K–562), compound **3f** showed excellent

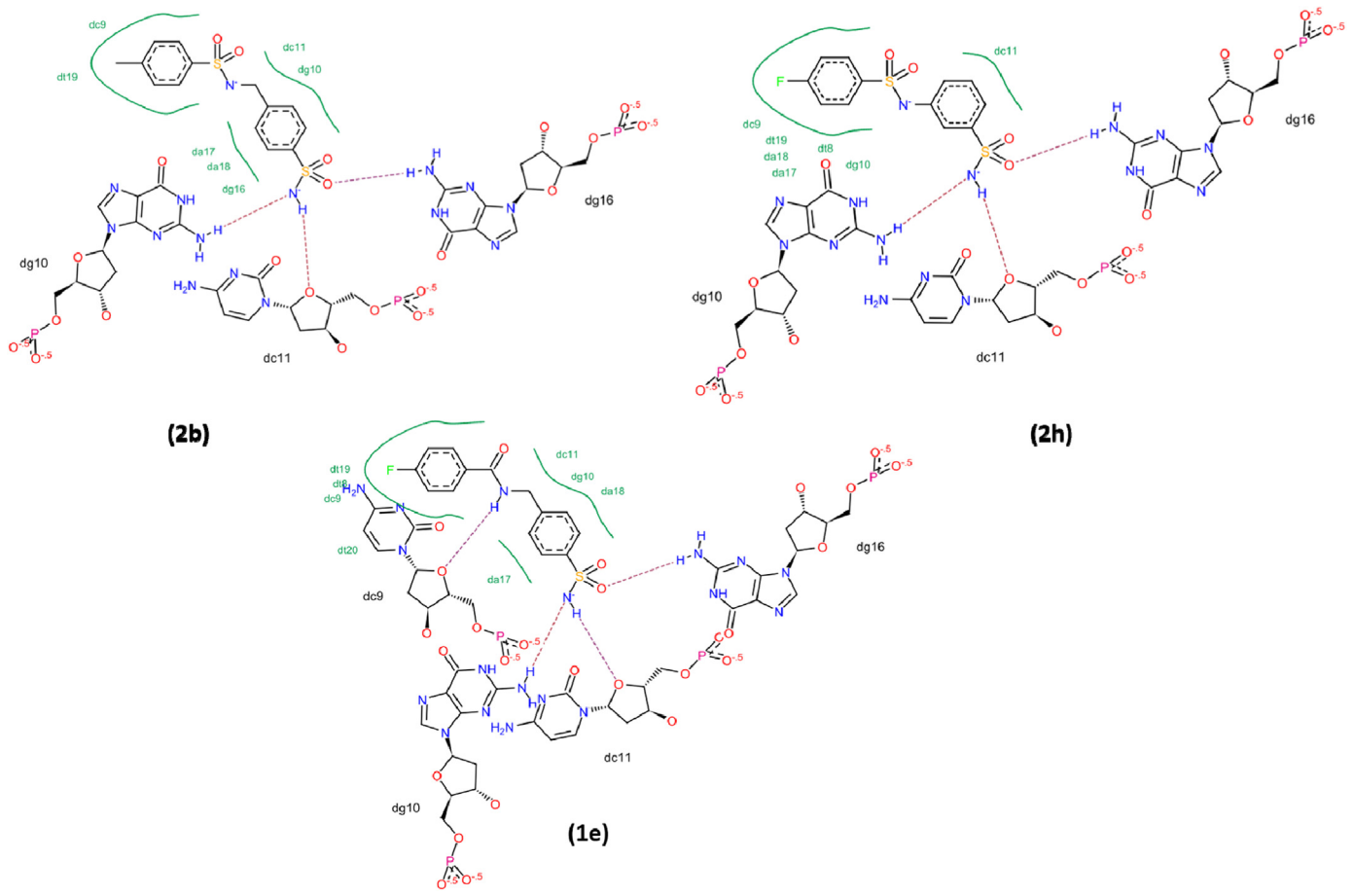


**Fig. 9.** 2D DNA-docked conformations of compounds **2b**, **2h** and **1e**.

growth inhibition of 98%, followed by compound **3e** that showed 90% inhibition. Compounds **3a** and **3c** were also found to be potent anticancer agents exhibiting 80% and 84% growth inhibition respectively. Against cervical cancer cells (HeLa), compound **3b** exhibited maximum growth inhibition of 77%. Compounds **3a** and **3j** exhibited 72% inhibition, followed by compound **3c** that showed 70% inhibition.

Similar to the results obtained for previous compounds (**1a**-**1g**, **2a**-**2k**), all 1*H*–pyrazol–4–yl benzamides (**3a**-**3j**) also did not inhibit growth of normal/healthy baby hamster kidney cells (BHK–21). In the quest to design new potent anticancer agents, the ability of anticancer compounds to selectively inhibit the growth of only cancerous cells, and not healthy cells is of utmost importance (Fig. 2). Hence compounds from this series present attractive lead molecules for further development as anticancer agents.

Next we performed flow cytometric analysis in order to determine whether or not the tested compounds had the ability to affect the cell cycle and induce apoptosis. The flow cytometric method is based on analysis of cellular DNA content, which was stained with fluorescent DNA binding dye, propidium iodide (PI). The selected derivatives were treated at final concentration of 100 μM with respective cell line i.e. MCF–7, K–562 or HeLa. The compounds **2b** and **3i** exhibited 58.1% and 57.6% apoptosis in MCF–7 cell line (Figs. 3 and 4). The detailed cell cycle analysis suggests that these compounds interfere with, and inhibit the mitotic spindling that ultimately results in DNA damage and cell arrest in G2 phase. The G2 phase is a period of rapid cell growth where the cell prepares itself for the next stage, mitosis. Concerted interplay between a number of important proteins (PLK1, CHK1, Wee1, CDC25C and CDK1) determine successful conclusion of G2 checkpoint, these proteins are strongly influenced by DNA damage and repair signaling (Gooijer et al., 2017).

When the effect was observed against K–562 cells, the test compounds **2h** and **3f** were found to induce comparable apoptosis (53.5%) with respect to positive control, carboplatin (58.1%). The cell cycle analysis suggested that more cell death occurred in S phase as compared to other two phases (Go and G2). DNA replication is the hallmark event in S phase. It is crucial that during cell replication, identical copies of DNA be made with minimum or no errors. During this phase any damage to DNA is detected and a cascade of tightly regulated events is started that attempts to repair the damaged DNA. While this repair mechanism is going on, mitosis and cell replication is put on hold. In case of failure to repair the damaged DNA, cell death mechanisms are initiated (Branzei et al., 2005). Against human cervical cancer cells (HeLa), the compound **3b** induced maximum apoptosis (33.4%), while compound **1e** induced approximately 22.2% apoptosis. Compound **3b** was found to be the most effective with respect to S phase apoptotic cell death. In comparison to **1e** derivative, **3b** possessed more apoptotic activity with more cell arrest or accumulation of cell population in S phase (Fig.s 3 and 4). Thus the percentage of apoptotic cells with respect to the total cell count revealed that the compound **3b** induced significantly higher pro–apoptotic activity than **1e**, which correlates with the results obtained in the MTT assay (Figs. 1 and 2).

In order to support the results (DNA damage) obtained from flow cytometry, cell nucleus morphology was investigated 24 h after treatment of cancerous cells (MCF-7, K–562 and HeLa cells) with selected test compounds at 100 μM concentration using DAPI (4′,6-diamidino-2-phenylindole) and PI (propidium iodide) staining followed by observation using fluorescence microscopy. For comparison untreated MCF-7, K–562 and HeLa cells were was stained and observed under fluorescence microscope, carboplatin treated cells were used as control. The microscopic images with DAPI staining (Fig. 5(a)) show bluish

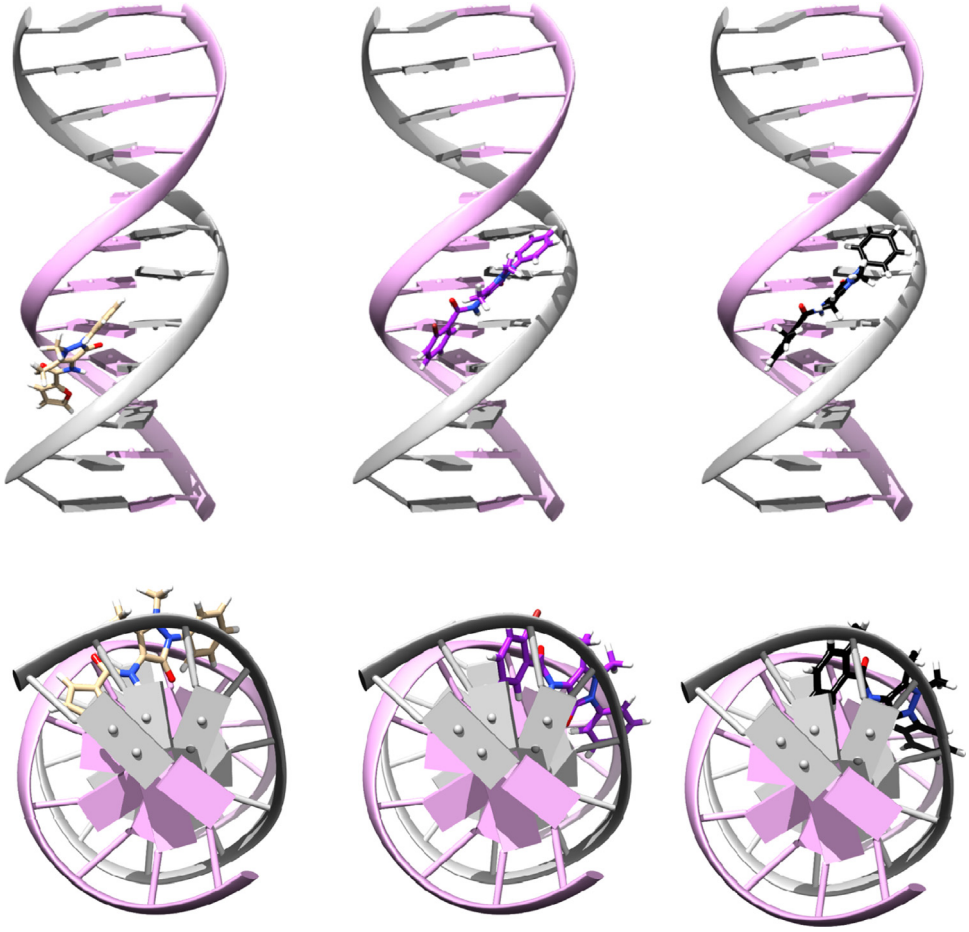

**Fig. 10.** Docked conformations of **3i** (tan), **3f** (purple) and **3b** (black), indicating DNA groove binding mode.

intact nuclei in the control and bright fragmented nuclei in cells treated with derivatives **2b, 3i, 2h, 3f, 1e** and **3b**. Similarly another dye, PI is impermeable to nuclei of living cells because of intact nuclear membrane. While in dead cells, the nuclear membrane is compromised that allows the permeability of PI with resultant image of red nuclei in front of black background (Fig. 5(b)). Among all the tested compounds, **2b, 3f,** and **3b** induced maximum apoptosis as indicated by DAPI and PI stained images in their respective cell lines (MCF-7, K-562 and Hela respectively), as compared to carboplatin, positive control. The results were in correlation with the flow cytometric analysis and suggested that there is a significant increase in DNA damage in each case. While other derivatives exhibited comparatively less apoptotic activity.

Since our investigation strongly suggested DNA damage to contribute to the observed apoptosis, we decided to carry out detailed DNA interaction studies. Small molecules can bind to and damage DNA in different ways, either via electrostatic interactions, or by binding in the major or minor groove of the DNA, or by intercalating in between the DNA base pairs. Cell death is triggered if DNA repair mechanisms fail or are compromised. The absorption spectra of test compounds in the absence and presence of increasing concentration of SS–DNA was observed as depicted in Fig.s 6 and 7. In each case of DNA interaction studies, with the increase in DNA concentration, a corresponding increase in the intensity of absorption bands at 220 nm and 260 nm was observed (hyperchromic effect), with no shift in the position of the bands, which remained unaffected by increase in concentration of SS-DNA. The hyperchromic effect indicates the non–covalent, groove binding interaction with DNA (Sirajuddin et al., 2014). Binding constants were determined using Benesi–Hildebrand's equation which is given below (Benesi and Hildebrand, 1949).

$$\frac{A_0}{A - A_0} = \frac{\varepsilon_G}{\varepsilon_{H-G} - \varepsilon_G} + \frac{\varepsilon_G}{\varepsilon_{H-G} - \varepsilon_G} \times \frac{1}{K\,[\mathrm{DNA}]}$$

Where K is the association/binding constant, Ao and A are the absorbance of the compound and its complex with DNA, respectively, and $\varepsilon_G$ and $\varepsilon_{H\text{-}G}$ are the absorption coefficients of the compound and compound–DNA complex, respectively. The binding constants (K) were obtained from the intercept-to-slope ratios of Ao/(A-Ao) vs. 1/[DNA] plots. The Gibbs free energy (ΔG) was determined from the following equation, where R is the general gas constant (8.314 $JK^{-1}$ $mol^{-1}$), and T is temperature (298 K).

$$\Delta G = -RT \ln K$$

The binding constant K for compounds **2b**, **2h** and **1e** were calculated to be $8.52 \times 10^2$ $M^{-1}$, $11.31 \times 10^2$ $M^{-1}$, and $19.80 \times 10^2$ $M^{-1}$ respectively in the order **2b** < **2h** < **1e**. The corresponding Gibbs free energies (ΔG) were found to be − 17.48 kJ/mol, − 17.16 kJ/mol and − 17.88 kJ/mol respectively. Similar results were obtained for 1*H*–pyrazol–4–yl benzamides **3i**, **3f** and **3b** (Fig. 7). Upon increasing the concentration of added DNA, an increase in the intensity of absorption bands at 220 nm and 260 nm was observed (hyperchromic effect), whereas the absorption bands did not shift their position, indicating groove binding as the mechanism responsible for observed DNA interaction (Fig. 8). Maximum binding constant was observed for compound **3b** ($K = 10.15 \times 10^2$ $M^{-1}$, $\Delta G = -17.87$ kJ/mol).

Groove binding interaction was stabilized by formation of hydrogen bonds between the compounds and the DNA base pairs. As can be seen from Fig. 9, compounds **2b**, **2h** and **1e** have identical binding pattern, where the sulfonamide NH group was making hydrogen bonds with guanine (dg 10) and cytosine (dc11), one of the sulfonamide oxygen

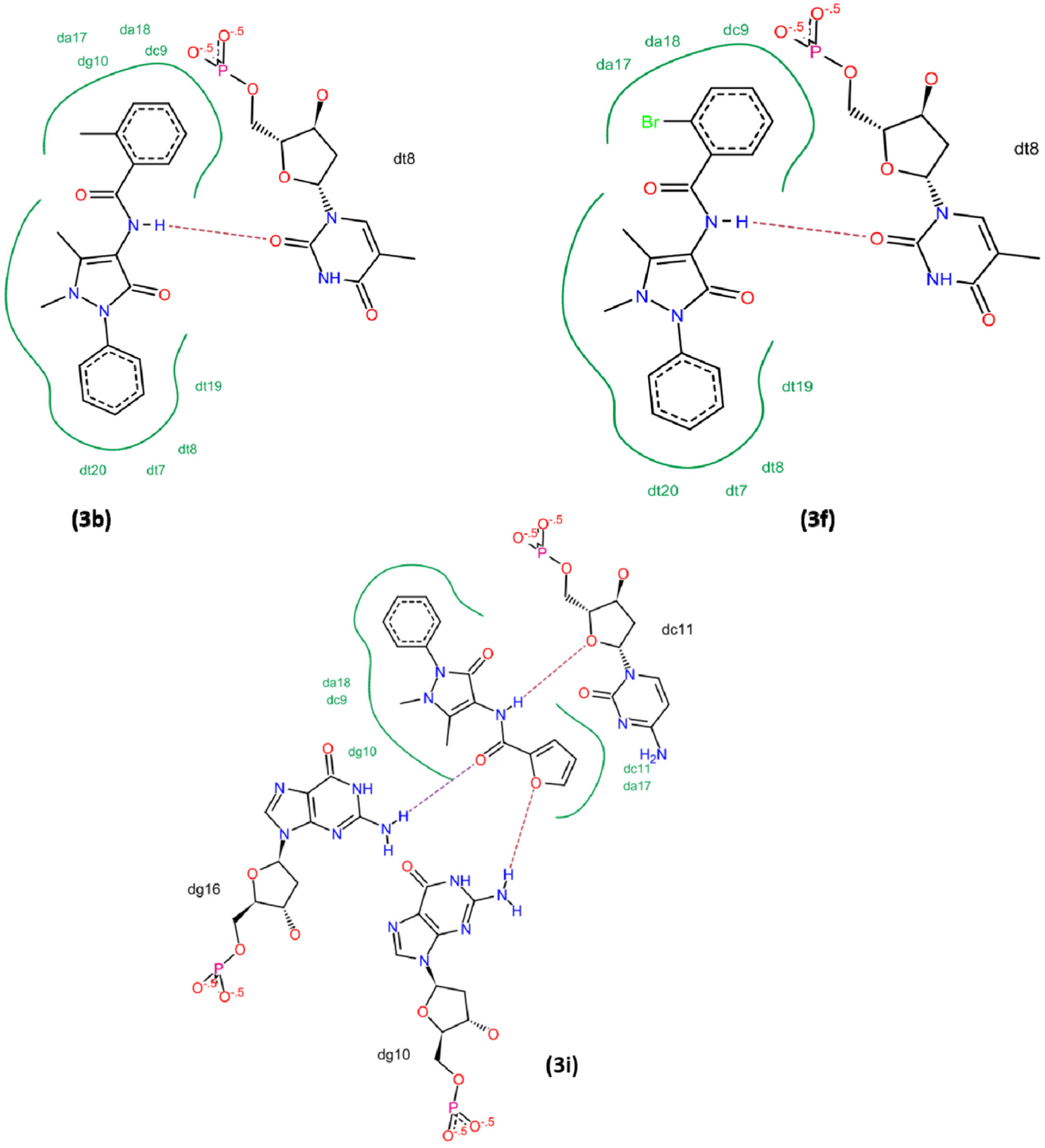


**Fig. 11.** 2D DNA-docked conformations of compounds **3b**, **3f** and **3i**.

was making a hydrogen bond with another guanine (dg16) (Fig. 9). Similar results were obtained from docking of 1*H*–pyrazol–4–yl benzamides **3i**, **3f** and **3b**, as shown in Fig. 10. All docked conformations indicated goove binding mode of interaction with the DNA, which is in agreement with the experimental data. From docking studies, it was evident that all compounds bind in the minor groove of the DNA (Fig. 10). Hydrogen bonded interactions with the DNA base pairs were also observed (Fig. 11). Compounds **3b** and **3f** had identical binding modes, contrary to sulfamoyl benz(sulfon)amides, these two compounds prefer to bind in AT rich region, as indicated by hydrogen bond formation between the NH of amide group and carbonyl oxygen of thymine (dt8). However compound **3i** was found to bind in GC rich region, due to the presence of furan group, which is absent in other compounds. The NH amide group was making a hydrogen bond with cytosine (dc11), whereas the carbonyl oxygen of amide group was making a hydrogen bond with amino group of guanine (dg16). The

furan ring oxygen was also making a hydrogen bond with amino group of another guanine (dg10) (Fig. 11).

If DNA damage is responsible for observed anticancer activity, as our investigations suggest, it can very well be anticipated that similar DNA binding and damage processes could also be going on for normal healthy cells (as indicated by MTT test against normal BHK-21 cells), why is it then that our tested compounds did not inhibit growth of normal BHK-21 cells? This can be explained by looking at the results obtained from flow cytometry, indicating that compounds **2b** and **3i** cause cell arrest in G2 phase (preceding mitosis), while all other tested compounds indicated cell arrest in S phase (preceding G2 phase). Since cancer cells are undergoing rapid cell division as compared to the normal cells, this makes them much more susceptible to such cytotoxic compounds. Furthermore, normal cells have active DNA damage detection and repair mechanisms, which are either impaired, or have been compromised in cancerous cells.

## 5. Conclusion

Sulfamoyl benz(sulfon)amides **(1a-1g, 2a-2k)** and 1*H*–pyrazol–4–yl benzamides **(3a-3j)** were evaluated for their anticancer potential against MCF–7, K–562 and HeLa cancer cell lines. Majority of the derivatives exhibited excellent cytotoxic activity against cancer cells, while showing insignificant cytotoxicity against the normal cell line (BHK–21), indicating that these compounds can be good candidates to be developed further as anticancer drugs. Among sulfamoyl benz(sulfon)amides, compounds **2b, 2h** and **1e** exhibited excellent growth inhibition against MCF–7, K–562 and HeLa cancer cells, respectively. Similarly among 1*H*–pyrazol–4–yl benzamides, compounds **3i, 3f** and **3b** were found to be most active against MCF–7, K–562 and HeLa cancer cells, respectively. Compounds **2b** and **3i** exhibited 58.1% and 57.6% apoptosis in MCF–7 cell line. Detailed cell cycle analysis suggested that these compounds interfere with, and inhibit the mitotic spindling which eventually results in DNA damage and cell arrest in G2 phase. Against K–562 cells, compounds **2h** and **3f** induced 53.5% apoptosis. Cell cycle analysis suggested that more cell death occurred in S phase as compared to other two phases (G0 and G2). Against human cervical cancer cells (HeLa), compound **3b** induced maximum apoptosis of 33.4%, while compound **1e** induced 22.2% apoptosis. The results from fluorescence microscopic analysis complemented these results. DNA interaction study using UV–visible spectroscopy indicated significant binding with DNA, with groove binding as the preferred mode of binding with DNA. To further rationalize binding interactions, DNA docking studies were carried out, confirming that compounds bind in the minor groove of the DNA.

## Acknowledgments

The authors are grateful to the Organization for the Prohibition of Chemical Weapons (OPCW), The Hague, The Netherlands and Higher Education Commission of Pakistan for the financial support through Project No. 20-3733/NRPU/R&D/14/520.

## References

Alegaon, S.G., Alagawadi, K.R., 2012. New thiazolidinedione-5-acetic acid amide derivatives: synthesis, characterization and investigation of antimicrobial and cytotoxic properties. Med. Chem. Res. 21, 816–824.

al-Rashida, M., Ahsen, S., 2015. In search of a docking protocol to distinguish between DNA intercalators and groove binders: genetic algorithm vs. shape-complementarity based docking methods. RSC Adv. 5, 72394–72404.

al-Rashida, M., Ejaz, S.A., Ali, S., Shaukat, A., Hamayoun, M., Ahmed, M., Iqbal, J., 2015. Diarylsulfonamides and their bioisosteres as dual inhibitors of alkaline phosphatase and carbonic anhydrase: structure activity relationship and molecular modelling studies. Bioorg. Med. Chem. 23, 2435–2444.

Aly, H.M., El-Gazzar, M.G., 2012. Novel pyrazole derivatives as anticancer and radiosensitizing agents. Arzneimittelforschung 62, 105–112.

Ban, J.O., Jung, Y.S., Kim, D.H., Park, K.R., Yun, H.M., Lee, N.J., Lee, H.P., Shim, J.H., Jeong, H.S., Lee, Y.H., Ham, Y.W., 2014. (E) − 2, 4-Bis (p-hydroxyphenyl) − 2-butenal inhibits tumor growth via suppression of NF-κB and induction of death receptor 6. Apoptosis 19, 165–178.

Benesi, H.A., Hildebrand, J.H., 1949. A spectrophotometric investigation of the interaction of iodine with aromatic hydrocarbons. J. Am. Chem. Soci. 71 (2707.27).

Branzei, D., Foiani, M., 2005. The DNA damage response during DNA replication. Curr. Opin. Cell Biol. 17, 568–575.

Bhatt, A., Kant, R., Singh, R.K., 2016. Synthesis of some bioactive sulfonamide and amide derivatives of piperazine incorporating imidazo [1, 2-B] pyridazine moiety. Med. Chem. 6, 257–263.

Danaei, G., Vander Hoorn, S., Lopez, A.D., Murray, C.J., Ezzati, M., 2005. Causes of cancer in the world: comparative risk assessment of nine behavioural and environmental risk factors. Lancet 366, 1784–1793.

Drew, H.R., Wing, R.M., Takano, T., Broka, C., Tanaka, S., Itakura, K., Dickerson, R.E., 1981. Structure of a B-DNA dodecamer: conformation and dynamics. Proc. Natl. Acad. Sci. USA 78, 2179–2183.

Dutta, A.S., Garner, A., 2003. The pharmaceutical industry and research in 2002 and beyond. Drug News Perspect. 16, 637–639.

Faria, J.V., Vegi, P.F., Miguita, A.G.C., dos Santos, M.S., Boechat, N., Bernardino, A.M.R., 2017. Recently reported biological activities of pyrazole compounds. Bioorg. Med. Chem. 25, 5891–5903.

Fortin, S., Bérubé, G., 2013. Advances in the development of hybrid anticancer drugs. Expert Opin. Drug Discov. 8, 1029–1047.

Ghorab, M.M., Alsaid, M.S., Nissan, Y.M., 2014. Synthesis and molecular docking of some novel anticancer sulfonamides carrying a biologically active pyrrole and pyrrolopyrimidine moieties. Acta Pol. Pharm. 71, 603–614.

Ghorab, M.M., Ragab, F.A., Heiba, H.I., Soliman, A.M., 2016. Design and synthesis of some novel 4-Chloro-N-(4-(1-(2-(2-cyanoacetyl) hydrazono) ethyl) phenyl) benzenesulfonamide derivatives as anticancer and radiosensitizing agents. Eur. J. Med. Chem. 117, 8–18.

Ghorab, M.M., Ragab, F.A., Heiba, H.I., El-Gazzar, M.G., Zahran, S.S., 2015. Synthesis, anticancer and radiosensitizing evaluation of some novel sulfonamide derivatives. Eur. J. Med. Chem. 92, 682–692.

Gooijer, M.C., Top, A., Bockaj, I., Beijnen, J.H., Würdinger, T., Tellingen, O., 2017. The G2 checkpoint—a node-based molecular switch. FEBS Open Bio. 7, 439–455.

Kateb, B., Chiu, K., Black, K.L., Yamamoto, V., Khalsa, B., Ljubimova, J.Y., Ding, H., Patil, R., Portilla-Arias, J.A., Modo, M., Moore, D.F., 2011. Nanoplatforms for constructing new approaches to cancer treatment, imaging, and drug delivery: what should be the policy? Neuroimage 54, S106–S124.

Kouatly, O., Geronikaki, A., Kamoutsis, C., Hadjipavlou-Litina, D., Eleftheriou, P., 2009. Adamantane derivatives of thiazolyl-N-substituted amide, as possible non-steroidal anti-inflammatory agents. Eur. J. Med. Chem. 44, 1198–1204.

LeadIT, 2014. at ⟨http://www.biosolveit.de/LeadIT/⟩.

Liu, J.J., Zhao, M.Y., Zhang, X., Zhao, X., Zhu, H.L., 2013. Pyrazole derivatives as antitumor, anti-inflammatory and antibacterial agents. Mini-Rev. Med. Chem. 13, 1957–1966.

MOE, version, 2014. 0901, Chemical Computing Group (CCG), Montreal, Canada, ⟨http://www.chemcomp.com/MOEMolecular_Operating_Environment.htm⟩.

Mosmann, T., 1983. Rapid colorimetric assay for cellular growth and survival: application to proliferation and cytotoxicity assays. J. Immunol. Methods 65, 55–63.

Nepali, K., Sharma, S., Kumar, D., Budhiraja, A., Dhar, K.L., 2014a. Anticancer hybrids-a patent survey. Recent Pat. Anti-Cancer Drug Discov. 9, 303–339.

Nepali, K., Sharma, S., Sharma, M., Bedi, P.M.S., Dhar, K.L., 2014b. Rational approaches, design strategies, structure activity relationship and mechanistic insights for anticancer hybrids. Eur. J. Med. l Chem. 77, 422–487.

Nikš, M., Otto, M., 1990. Towards an optimized MTT assay. J. Immunol. Methods 130, 149–151.

Rakesh, K.P., Wang, S.M., Jing, L., Ravindar, L., Asiri, A.M., Marwani, H.M., Qin, H.L., 2017. Recent development of sulfonyl or sulfonamide hybrids as potential anticancer agents: a key review. Anticancer Agents Med. Chem. http://dx.doi.org/10.2174/1871520617666171103140749.

Saeed, A., Ejaz, S.A., Khurshid, A., Hassan, S., al-Rashida, M., Latif, M., Lecka, J., Sévigny, J., Iqbal, J., 2015. Synthesis, characterization and biological evaluation of N-(2, 3-dimethyl-5-oxo-1-phenyl-2, 5-dihydro-1H-pyrazol-4-yl) benzamides. RSC Adv. 5, 86428–86439.

Saito, Y., Uchida, N., Tanaka, S., Suzuki, N., Tomizawa-Murasawa, M., Sone, A., Najima, Y., Takagi, S., Aoki, Y., Wake, A., Taniguchi, S., 2010. Induction of cell cycle entry eliminates human leukemia stem cells in a mouse model of AML. Nat. Biotechnol. 28, 275–280.

Scozzafava, A., Owa, T., Mastrolorenzo, A., Supuran, C.T., 2003. Anticancer and antiviral sulfonamides. Curr. Med. Chem. 10, 925–953.

Sirajuddin, M., Ali, S., McKee, V., Zaib, S., Iqbal, J., 2014. Organotin (IV) carboxylate derivatives as a new addition to anticancer and antileishmanial agents: design, physicochemical characterization and interaction with Salmon sperm DNA. RSC Adv. 4, 57505–57521.

Soni, B., Ranawat, M.S., Sharma, R., Bhandari, A., Sharma, S., 2010. Synthesis and evaluation of some new benzothiazole derivatives as potential antimicrobial agents. Eur. J. Med. Chem. 45, 2938–2942.

Visualizer, D.S. 2005. Accelrys Software Inc, Discovery Studio Visualizer, 2.